2009

Influence of surface states on tunneling spectra of n-type GaAs(110) surfaces

Nobuyuki Ishida
Hokkaido University

Kazuhisa Sueoka
Hokkaido University

Randall M. Feenstra
Carnegie Mellon University, feenstra@andrew.cmu.edu

Follow this and additional works at: http://repository.cmu.edu/physics

Influence of surface states on tunneling spectra of *n*-type GaAs(110) surfaces

Nobuyuki Ishida,[1] Kazuhisa Sueoka,[1] and R. M. Feenstra[2,*]

[1]*Graduate School of Information Science and Technology, Hokkaido University, Kita 14, Nishi 9, Kita-ku, Sapporo 060-0814, Japan*
[2]*Department of Physics, Carnegie Mellon University, Pittsburgh, Pennsylvania 15213, USA*

We show that surface states within the conduction band of *n*-type GaAs(110) surfaces play an important role in reducing the tunneling current out of an accumulation layer that forms due to an applied potential from a nearby probe tip. Numerical computation of the tunneling current combined with an electrostatic potential computation of the tip-induced band bending (TIBB) reveals that occupation of the surface states limits the TIBB, thus leading to the limitation of the accumulation. As a result, the tunneling current out of the accumulation layer is strongly suppressed, which is in quantitative agreement with the experiment.

PACS number(s): 73.20.At, 68.37.Ef, 73.25.+i

I. INTRODUCTION

Since the invention of scanning tunneling microscopy (STM), scanning tunneling spectroscopy (STS) has been recognized as an essential part of STM and continuing efforts to improve the experimental and analytical methods have been made.[1–4] Normally, tunneling conductance is interpreted as a quantity that is proportional to the local density of states at surfaces and observed features in the spectra are related to the states at an energy E with a simple relationship $E-E_F = eV$, where E_F is the Fermi level in the sample and V is the sample-tip voltage. In the case of STS on semiconductor surfaces, however, so-called tip-induced band bending (TIBB) modify the relationship into $E-E_F = eV - \phi_0$, where ϕ_0 is the TIBB at the surface [Fig. 1(a)]. Although this formula is suitable for the tunneling conductance arising from surface states, this simple picture cannot be applied for the tunneling conductance arising from bulk states due to the additional quantum effects as depicted in Figs. 1(b) and 1(c). These effects make it complicated to interpret the spectra obtained on the semiconductor surfaces with a low surface-state density, such as the (110) surfaces of III–V semiconductors. To date, STS studies on the GaAs(110) surfaces have played an important role in the understanding of these effects and quantitative interpretation of the tunneling spectra.[1,2,5,6] But despite the extensive studies on this surface, detailed understanding of the tunneling spectra, particularly under accumulation conditions [Fig. 1(c)], has not yet been achieved.

In early STS work on the *n*-type GaAs(110) surface, tunneling current was observed at the bias range corresponding to the fundamental band gap. This current was recognized as arising from occupation of conduction-band (CB) states (extended or localized at the surface) due to electrons from dopant atoms and it was thus named as the "dopant-induced" component or D component.[1] However, a theoretical computation of the tunneling current employing free-electron effective-mass bands predicted that the tunneling current out of localized states formed in the surface accumulation layer was orders of magnitude larger than that found in the experiment. This discrepancy between the theory and experiment was not well understood at that time and the question of why the tunneling current out of the accumulation layer was

somehow suppressed in the experiments remained unresolved for years. In 2003, Jäger *et al.*[6] proposed an explanation for this issue by considering the role of the surface states within the CB, which is related to the momentum dependence of the tunneling probability; since the surface states within the CB are located at the $\bar{X}$ point of the surface Brillouin zone, the wave vector **k** has nonzero momentum parallel to the semiconductor surface (unlike the wave function at the $\bar{\Gamma}$ point). For this reason, the wave function of the surface states have a higher decay constant in the vacuum region[7] and hence a low tunneling probability. It is known for GaAs(110) that the unoccupied surface band is resonant with the CB (slightly above the CB minimum)[8] and Jäger *et al.*[6] argued that mixing of the accumulation layer states would occur with the surface band thereby producing low tunneling probability for the accumulation states. Although they supplied this *qualitative* explanation of the tunneling spectra and bias dependence of the topographic images by considering the role of the surface states, a *quantitative* explanation of the spectra was not attempted. In this work, we follow Jäger *et al.* in considering the influence of surface states on the tunneling spectra but we consider a separate role of the surface states that was not explored in their discussion, namely, the effect of the *occupation* of the states on the TIBB.
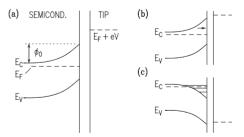

FIG. 1. (a) Schematic diagram of energy bands with a varying electrostatic potential (TIBB), showing the valence-band maximum E_V and the conduction-band minimum E_C. The sample Fermi level is denoted by E_F with the tip Fermi level at $E_F + eV$ where V is the sample-tip voltage. The band bending at the surface is denoted by ϕ_0. Quantum effects within the semiconductor are illustrated in (b) and (c) for wave-function tailing through a depletion region and for localized accumulation state formation, respectively.

In our work, we perform STS on the *n*-type GaAs(110) surface and we compare the results with a numerical computation of tunneling current combined with an electrostatic potential computation of the TIBB. In the potential computation, we treat surface charges arising from occupation of the surface states within the CB. The theory reveals that the TIBB at negative voltages is limited by occupation of the surface states (so-called surface pinning), which in turn leads to a drastic limitation of the electron accumulation. As a result, the tunneling current out of the accumulation layer is strongly suppressed, which is in quantitative agreement with the experiment. Also, we show, by comparing this computation with the one taking into account the low tunneling probability explained above that the surface pinning due to the occupation of the surface states has a major effect in reducing the current out of the CB, rather than the low tunneling probability.

This paper is organized as follows. Experimental and computational details are summarized in Secs. II and III, respectively. In Sec. IV, a tunneling spectrum from the experiment is presented and briefly explained, and then curve fitting of the theory with the experiment is performed in order to examine the effect of including the surface charge arising from the surface states. In Sec. V, we discuss possible effects that contribute to both the suppression of the CB current and broadening of the onset of the surface-state band. Also, we discuss the reasoning behind our neglect of the tunneling current through the assumed surface states themselves in our computation. Finally, we summarize our results.

II. EXPERIMENT

STS measurements are performed under the ultrahigh vacuum condition with a pressure less than 5×10^{-11} Torr. Commercial Pt-Ir tips are used. Tip cleaning is performed *in situ* using electron bombardment. An *n*-type GaAs(001) wafer (Si doped, $N_D = 1.0 \times 10^{18}$ cm^{-3}) is cleaved *in situ* to obtain a clean GaAs(110) surface. Tunneling spectra are acquired at room temperature using a voltage modulation of 50 mV and employing a lock-in amplifier to obtain differential conductance. The variable tip-sample separation technique is used to obtain large dynamic range of conductance, which is required for detecting the D component with a high S/N ratio.[2] The offset of the tip-sample separation has the form $\Delta s(V) = a|V|$ where V is the voltage applied to the sample relative to the tip and a is the proportionality coefficient with a typical value of 0.1 nm/V. The obtained spectra are converted to the constant tip-sample separation by multiplying the measured conductance by $\exp(2\kappa\Delta s)$ where a value of κ is determined experimentally from measurements of the tip-sample distance dependence of the tunneling current (a voltage-averaged value of 8 nm^{-1} is used for the data presented below).[2]

III. DETAILS OF THE COMPUTATION

Tunneling current is computed with a theory previously described.[9,10] The theory consists of a three-dimensional (3D) treatment of TIBB in the semiconductor[11] and a planar computation of tunneling current (using only the potential variation along the central axis of the problem) based on the Bardeen formalism.[12] In addition to the previously developed computation techniques for the 3D potential computation,[10,11,13,14] we have extended the technique to include a self-consistent solution of the coupled Poisson and Schrödinger equations, as needed for the present situation of accumulation at the surface. This extension is detailed in the Appendix. To incorporate the surface charges arising from occupation of the surface states, acceptor-type surface states having a Gaussian density distribution in energy within the CB are included in the electrostatic potential computation. Note that an acceptor(donor)-type surface state is negatively (positively) charged when it is occupied (empty) and neutral when empty (occupied). Since the surface states within the CB originate from the dangling bonds of the surface Ga atoms,[15] the spatial density is chosen to be 4.4×10^{14} cm^{-2}.

Strictly speaking, the surface states lying within the valence band (VB) or CB are resonant with the bulk states and thus the wave function is not completely localized at the surface but decays asymptotically through a subsurface region and has a small amplitude in the bulk. Although this tailing of the wave function is neglected in this computation, we believe that small adjustments of the parameters related to the acceptor-type surface states, that is, the energy position and full width at half maximum (FWHM) of the Gaussian distribution could accommodate this effect. As is well known, donor-type surface states also exist for the GaAs(110) surface, within the VB. We have also incorporated those in our computation but they play no role at all since they are never occupied with holes (these states might play a role, however, for *p*-type GaAs).

In addition to the semiconductor parameters such as doping concentration and effective mass, our computation contains parameters of the tip-sample separation, s, the tip radius, R, and the contact potential difference between the semiconductor and the probe tip, $\Delta\phi$. For the surface states, the energy position of the Gaussian distribution (defined as an energy difference between the centroid of the Gaussian distribution and the VB maximum), E_{SS}, and the FWHM, ΔE_{SS} are introduced as input parameters. For the semiconductor, three VBs (light hole, heavy hole, and split off bands) and a single CB are considered. We use the effective masses (in units of the free-electron mass) of 0.0635 for the CB, 0.084, 0.643, and 0.172 for the light, heavy, and split off VBs, and a spin-orbit splitting of 0.341 eV.[16] Wave function tailing through the semiconductor depletion region as well as localized states forming at the semiconductor surface, as depicted in Figs. 1(b) and 1(c), respectively, are fully accounted for.[9]

IV. RESULTS

A. Tunneling spectrum

A typical tunneling conductance spectrum from the *n*-type GaAs(110) surface is shown in Fig. 2(a) by the solid line. Three regimes of tunneling current are observed as in the previous work;[2] a component turning on at about 0 V and extending to positive voltages, a component turning on at
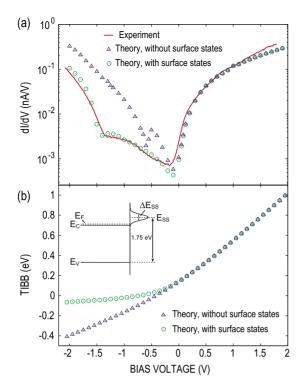
FIG. 2. (Color online) (a) Tunneling spectra of the *n*-type GaAs(110) surface from the experiment and theory. Solid line shows the experimental data. Open circles and triangles show the theoretical computation with and without inclusion of the surface states, respectively. (b) TIBB as a function of bias voltage computed with a 3D potential computation with (open circles) and without (open triangles) including the surface states. The TIBB is measured relative to the potential energy at a point far inside the semiconductor. The inset shows the density distribution of the surface states assumed in this computation.
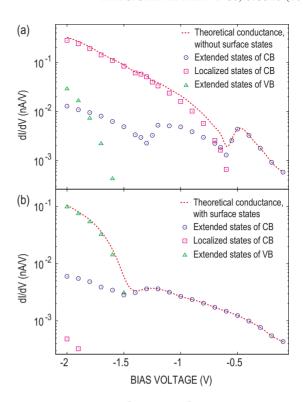

FIG. 3. (Color online) [(a) and (b)] Each component of the tunneling conductance computed with [in (b)] and without [in (a)] the surface states. Dotted lines show the total conductance. Open circles and squares show the conductance from the extended and localized states of the CB, respectively. Open triangles show the conductance from the extended states of the VB.

about −1.4 V and extending to negative voltages, and a shoulder existing in a range from −1.4 to 0 V. The component observed at the positive voltage range arises from the current out of the filled states of the probe tip to the empty CB states of the sample. The component observed at the voltage range from −1.4 to 0 V is the D component, corresponding to current out of occupied CB states of the sample into empty states of the probe tip. Due to the onset of the tunneling current out of the filled VB states, the spectrum shows a sharp rise beginning at about −1.4 V and extending to lower voltages. In the following, we perform curve fitting of the theory with the experiment using two different computation schemes, that is, with and without the inclusion of surface charge arising from occupation of the surface states within the CB.

B. Curve fitting without including the surface states

To understand the detailed behavior of the tunneling conductance, it is important to consider them with the TIBB, therefore, let us first explain the bias dependence of the TIBB. In Fig. 2(b), the bias dependence is displayed with the open triangles. In this potential computation, the surface charges arising from the surface states are not included. We

use parameter values of 0.9 nm, 70 nm, and 0.43 eV for *s*, *R*, and $\Delta\phi$, respectively. The TIBB is almost linearly dependent on the bias voltage and the slope changes at the voltage where the bands are in a flat band condition (i.e., depending on the value of $\Delta\phi$). In the case of *n*-type semiconductors, TIBB in the bias range below the flat band condition is smaller than those in the bias range above it due to the additional screening effect of the accumulated electrons.

The tunneling spectrum computed according to the potential just described is shown in Fig. 2(a) by the open triangles. For positive voltages, fairly good agreement between the theory and experiment is achieved. In the negative voltage range, on the other hand, the theory shows a large deviation from the experiment, that is, a result much larger than the experiment, as was found in the previous works.[1,6]

To investigate the cause of this large deviation in detail, we decompose the tunneling conductance into its components arising from extended and localized states, as shown in Fig. 3(a). The tunneling conductance from the extended states of the CB (open circles) increases rapidly for small negative voltage varying from 0 to −0.5 V and then starts to saturate below −0.5 V. The rapid increase is responsible for the deviation from the experiment at these small voltages. In this voltage range, the bands are still bent upward and thus the electrons in the extended states feel a (repulsive) potential barrier in the semiconductor region. Consequently, the tunneling probability strongly depends on the TIBB. For voltages below (i.e., more negative) this range, the band

starts to bend downward, and therefore there is no barrier in the semiconductor region, leading to the small dependence of the tunneling probability on the TIBB. Below −0.6 V, the tunneling conductance from the localized states of the CB sets in and increase rapidly (open squares), leading to a very large deviation from the experiment. This increase occurs because the number of accumulated carriers in the localized states increases as the bias voltage decreases due to the associated increase in the TIBB. Since the electrons at the CB feel a lower vacuum barrier (by a band-gap energy) than those at the VB, the tunneling current out of the localized states at the CB dominates the total conductance. For this reason, the onset of the VB component (open triangles) is not visible in the total conductance curve (dotted line).

One additional feature apparent in Fig. 3(a) is the oscillations in the conductance of the extended states. Intuitively, the tunneling probability of the extended states in the CB these through the semiconductor region where the band is bent downward (corresponding to a potential well) might be thought to monotonically increase as the TIBB decreases. However, the computed tunneling conductance shows peaks, which turn out to originate from a combination of localized-state formation and the manner in which the extended states (over a range of energies) "fit" into the potential well. This phenomenon is explicitly illustrated in the Appendix by displaying wave-function values for the states.

C. Curve fitting with the surface states

Since the surface states within the CB (explained in Sec. III) affect the tunneling current through a change in the potential (or the TIBB), we first explain the effect of the surface states on the potential computation. The TIBB as a function of bias voltage is shown in Fig. 2(b) by the open circles. We use surface-state parameters of 1.75 and 0.25 eV for E_{SS} and ΔE_{SS}, respectively. The other parameters are kept the same as above. In contrast to the bias dependence without the surface states, the TIBB starts to be limited (surface pinning) for negative voltages as the surface-state band comes closer to the Fermi level. For positive voltage range, there is no effect of including the surface states.

The tunneling spectrum computed with surface states included is shown in Fig. 2(a) by the open circles. In this case, the theoretical values for the tunneling conductance in the band-gap region (D component) are strongly suppressed and the theory provides a reasonable fit to the experiment. Again, we decompose the tunneling conductance into its components from extended and localized states, as displayed in Fig. 3(b). The rapid increase in the conductance seen at small negative voltages when surface states were neglected is now absent since the TIBB changes only very slowly due to the surface pinning. Also, the oscillations in the conductance of the extended states are absent since the band edge does not reach the particular energy position at which this effect occurs. The tunneling conductance from the localized states of the CB is negligible over the entire voltage range considered here: a localized accumulation layer state first forms at about −1.3 V and electrons in this state contribute to the tunneling current below this bias voltage. However, the tunneling cur-
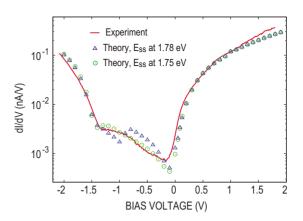

FIG. 4. (Color online) Dependence of the energy position of the surface state on the tunneling spectra. Solid line shows the experimental data. Open circles and triangles show the theoretical results with a E_{SS} value of 1.75 and 1.78 eV, respectively.

rent out of the state is three orders of magnitudes smaller than the current out of the extended states of the VB due to the limitation of the accumulation. Therefore, the only significant contribution to the tunneling conductance in the voltage range from −1.4 to 0 V is from the extended states of the CB. The extended states of the VB start to contribute at about −1.4 V, producing the onset of the large current component seen at this voltage, and they dominate the total conductance below this bias voltage.

It should be noted here that the formation of the localized accumulation layer states is sensitive to the parameters of the surface states, that is, E_{SS} and ΔE_{SS}. Experimentally, the energy position of the surface states was observed by inverse photoemission spectroscopy (IPES) to be about 1.75 eV with respect to the VB maximum.[8] Therefore, a E_{SS} value of 1.75 eV for the curve fitting is very reasonable. However, an increase in E_{SS} as small as 30 meV (which is within the experimental margin of error of the IPES result) appreciably affects the TIBB and the energy position at which the localized accumulation layer state first forms is changed to be −0.8 V. Importantly, even though the tunneling current out of the localized accumulation layer state starts to contribute from the smaller negative voltage, we find that, in comparison to the case without the surface states [Fig. 2(a), the open triangles], the theory still shows significant reduction in the conductance from the localized states and hence it gives a reasonable fit to the experiment as shown in Fig. 4 by the open triangles (although a modest deviation can be seen for small negative voltages). This fact suggests that the limitation of the accumulation arising from the limitation of the TIBB is important in order to explain the small D component seen in experiment, irrespective of the energy position of the formation of the localized accumulation layer state. To further investigate the formation of the localized states, more experiments are required especially at low temperatures, from which one could confirm the formation of quantum states from peaks in the spectra.[3,5] Additionally, we should note that the formation of localized quantum states may be dependent on the surface position where STS is performed since inhomogeneous potential fluctuations occur over the surface, as further discussed in the next section.
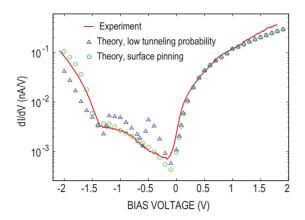
FIG. 5. (Color online) Comparison of the effect of the surface pinning with the low tunneling probability. Solid line is the experimental data. Open circles and triangles show the theoretical computation with taking into account the inclusion of either the surface pinning or the low tunneling probability arising from the momentum dependence, respectively.

V. DISCUSSION

A. Effect of the low tunneling probability

In essence, the role of the surface states in our computation is to limit the TIBB due to occupation of the states (surface pinning), which in turn limits the electron accumulation in the localized states of the CB. As a result, the tunneling current out of the localized states is strongly suppressed. Although the theoretical result is in good agreement with the experiment, we have to consider here the other effect that was proposed by Jäger *et al.* to explain the suppression of the D component, that is, the momentum dependence of tunneling probability.

To evaluate the possible effect of the low tunneling probability, we perform another computation with a different computation scheme; the surface states are not included in the potential computation (which means physically that occupation of those surface states is prohibited) and the tunneling current out of the localized states of the CB is set to be zero in order to simulate a low tunneling probability. The results are shown in Fig. 5 with open triangles together with the experimental data and the result where surface pinning is included. Although agreement between the theory and experiment is relatively poor, the computed tunneling spectrum again does reproduce the overall character of the experiment. One important difference between the computed spectra with and without the surface states, however, is the small but significant shift in the location of the VB onset (near −1.4 V) in the latter case. The TIBB is too large in the absence of occupation of the surface states to permit a quantitative description of the experimental data. If we change the parameter of $\Delta\phi$ to a higher value such as 0.6 eV, then the VB onset comes closer to −1.4 V but in that case the D component becomes much larger than the experiment, leading to large deviation. From this result, we conclude that the mechanism of Jäger *et al.* alone is insufficient to explain the data, whereas our model which takes into account the occupation of the surface states does provide a good fit to the data.

In any case, since the surface states undoubtedly exist within the CB (Ref. 8) and for *n*-type material there is no possible cause that could prohibit occupation of these states, their occupation is something that must be included in any theory (although the degree of localization of the surface states at the surface may affect the degree to which they constrain the TIBB). Therefore, we find that the limitation of the accumulation current at the CB due to occupation of the surface bands seems to have the major effect on the suppression of the CB current observed in the experiment. As a separate observation, we have found, based on experiments over many years using scores of samples and tips, there is an absolute maximum in the intensity of the D component, which is consistent with our model of surface pinning due to intrinsic surface states. In the case of the computation without the surface states, the intensity of the D component is strongly dependent on the parameter $\Delta\phi$ since it strongly affects the TIBB and the intensity of the D component using relatively low values of $\Delta\phi$ becomes larger than that in any experimental data. On the other hand, the dependence of the intensity of the D component on $\Delta\phi$ becomes much smaller in the computation with the surface states since the surface pinning strongly constrains the range of the TIBB at the negative bias ranges.

B. Broadening of the surface-state band

Another point that should be discussed concerns broadening of the edge of the surface-state band. In our computation, the energy position and the FWHM of the Gaussian distribution of the surface states are introduced as input parameters. We performed curve fitting of the theory to many different experimental spectra by varying these parameters as well as the other parameters (s, R, and $\Delta\phi$). For some data in which the VB onset is seen at slightly higher energy position than −1.4 V, a relatively lower energy of E_{SS} and/or a larger value of ΔE_{SS} are needed to obtain reasonable fits. Changing the other parameters (s, R, and $\Delta\phi$) is found to be ineffective in following the slight shifts in the VB onset of this kind. As opposed to the parameters of s, R, and $\Delta\phi$, the surface-state parameters might be thought of as having fixed values for all the curve fits since the surface states arises from the intrinsic properties of the surface. However, some variation in these parameters values can be explained by the consideration of inhomogeneous potential fluctuations occurring over the surface: Even if we prepare our samples in an ultrahigh vacuum condition, there still always exist defects, adsorbates, etc., which produce potential variations (as well as possibly producing extrinsic surface states) that affect the TIBB.[14] Since we tend to acquire our spectra relatively far from any extrinsic defects during the actual experiments, the features from the extrinsic states themselves are not usually seen in the spectra. However, they could affect the spectra through a change in the TIBB. In other words, the surface region that is actually constraining (pinning) the Fermi level could be far from the actual tip location where we are acquiring a spectrum. Considering these effects, we suppose that the spectra for which we need a relatively lower energy of E_{SS} and/or a larger value of ΔE_{SS} for the curve fitting might well be influenced by extrinsic defects.

C. Tunneling current through the surface states

The present computations employ free-electron effective-mass bands and hence no surface localization of the wave functions (other than through accumulation states) is present. Nevertheless, the computations do assume that presence of a surface band and charging of this band severely limits the TIBB. But, importantly, we do *not* include in the computations the possibility of any current flowing through these surface states. The relevant surface states are known to be resonant with the CB, lying near the CB minimum, and indeed in experimental STS spectra a small feature associated with the states is observed [this feature is also seen for the present data, if it is plotted as $(dI/dV)/(\overline{I/V})$].[2] STM images also reveal the presence of the states,[17] although for both the STS and STM data the signature of the surface states is found to depend somewhat on the probe tip and/or the position on the sample from which the spectra were acquired. Our rationale for neglecting the contribution from the surface states in our computed spectra is that the measured spectra reveal directly that this contribution is relatively small.[2] This small magnitude is not surprising since the states are localized near the $\overline{X}$ point and hence will have a low tunneling probability (i.e., following the arguments of Jäger *et al.*[6] but applying them in a slightly different manner than done by those authors).

A more complete description of the tunneling spectra of GaAs(110) would start from a more realistic description of the electronic states, e.g., employing a pseudopotential computation (as in Ref. 17) but fully including the band bending within the semiconductor. This description would be quite complex, since surface states will partially shift according to the potential at the surface but not completely so, since the states extend into the bulk. A full description of the quantum effects pictured in Figs. 1(b) and 1(c) within a framework that includes realistic surface states has not yet been achieved by any authors. For such a computation, and considering the accumulation regime, certainly the type of mixing between surface and bulk states discussed by Jäger *et al.*[6] will play some role in determining the tunnel current. However, we feel that we have demonstrated conclusively here that the occupation of the surface states plays a large (and dominant) role in suppressing the formation of the accumulation layer states.

VI. SUMMARY

In summary we have shown, following Jäger *et al.*,[6] that surface states play an important role in explaining the suppression of the tunneling current out of the localized accumulation layer states of the CB for spectra obtained from *n*-type GaAs(110) surfaces. Numerical computation of tunneling current combined with an electrostatic potential computation of the TIBB gives evidence that as the surface-state band comes closer to the Fermi level, electrons at the CB start to occupy the surface states and thus limit any further TIBB (i.e., surface pinning). As a result, electron accumulation in the localized states is strongly limited, which leads to the suppression of the tunneling current out of the CB states.

The computed tunneling spectrum shows quantitative agreement with the experiment. We also considered the effect of the low tunneling probability due to the momentum dependence for the cause of the suppressed accumulation layer current, as specifically suggested by Jäger *et al.* However, we find in this case that the position of the VB onset in the computed spectra does not match well with the experiment since the TIBB is too large. Thus, we find that the limitation of the accumulation at the CB due to the occupation of the surface states has the major effect in determining the magnitude of the observed tunnel current.

APPENDIX: SELF-CONSISTENT COMPUTATION OF 3D POTENTIAL

Computations are performed using a theory previously described,[9–11] along with some extensions as described below. The 3D electrostatic problem of a hyperbolic-shaped probe tip in proximity to a semiconductor is solved using a finite-element approach. This method successfully handles the highly nonlinear problem that occurs under conditions of carrier accumulation or inversion. Our implementation of the method has been validated by taking the solution and solving the inverse problem using the method of images. The finite-element grid consists of rectangular coordinates in the semiconductor (with increasing spacing of the grid as distance from the tip apex increases) and modified prolate spheroidal coordinates (designed to exactly match the tip shape[10]) in the vacuum. The problem has azimuthal (circular) symmetry. The result of the finite-element computation is the electrostatic potential energy, $\phi(r,z)$, where r is the radial coordinate and z extends into the semiconductor.

To obtain a tunnel current, a one-dimensional (1D) integral of the Schrödinger equation is computed along the central axis, $r=0$. This numerical integration is performed for all energies of interest, yielding the full set of extended and/or localized wave functions associated with the potential $\phi(0,z)$.[18] The current is then obtained from the wave functions evaluated at some distance (the tip-sample separation) out into the vacuum with those values employed in a planar tunneling computation.[10] Use of only a single 1D integral to obtain the states of interest is valid in situations when the radial variation in the potential is relatively small, which is satisfied for the cases of interest in the present work.

Our method has been successfully employed in prior studies for which the semiconductor was in depletion.[10] In that case the charge density for all z values can, to a good approximation, be evaluated from its semiclassical value,

$$\rho_C(r,z) = \rho_D[E_F - \phi(r,z)] + \rho_A[E_F - \phi(r,z)]$$
$$+ \rho_{CB}[E_F - \phi(r,z)] + \rho_{VB}[E_F - \phi(r,z)],$$
$$(A.1)$$

where ρ_D, ρ_A, ρ_{CB}, and ρ_{VB} are the charge densities due to donor impurities, acceptor impurities, CB, and VB, respectively, that would be computed for a spatially homogeneous bulk semiconductor [e.g., Eqs. (1)–(4) of Ref. 9]. Using the usual semiclassical approximation of band bending these charge densities, which are normally a function of Fermi-level position E_F, are now evaluated at $E_F - \phi(r,z)$.

For situations of accumulation or inversion, additional considerations are necessary. For a self-consistent solution, we must evaluate charge densities using the same wave functions employed in the computation of tunnel current. A general method for accomplishing this, and one that again employs a semiclassical approximation for the radial part of the wave function, is to compute additional 1D integrals that solve the Schrödinger equation at *each* of the radial coordinates r_i in the problem. Thus, for each potential curve $\phi(r_i,z)$ we obtain the associated wave functions $\psi_\mu(r_i,z)$ and energies ε_μ by numerical integration; these provide solutions for the z component of the problem. For the radial component we take the semiclassical wave functions, $\chi_{k_\parallel} = \exp(i\mathbf{k}_\parallel \cdot \mathbf{r})/\sqrt{A}$ (where A is a normalization area), with energies $\hbar^2 k_\parallel^2/2m^*$ where $\mathbf{k}_\parallel$ is the parallel component of the wave vector. The charge density in the Hartree approximation is obtained by a summation over all states of the charge per unit volume, $|\psi_\mu(r_i,z)\chi_{k_\parallel}(r)|^2(\pm e) = |\psi_\mu(r_i,z)|^2(\pm e)/A$, multiplied by the thermal occupation factor of each state. The sum over parallel wave vector yields simply $Am^*/(\pi\hbar^2)$, i.e., the density of states for a two-dimensional electron gas. The charge density for localized states, writing the result for states derived from a CB, is thus found to be

$$\rho_L(r_i,z) = \frac{(-e)m^*}{\pi\hbar^2} \sum_\mu |\psi_\mu(r_i,z)|^2 \int_{\varepsilon_\mu}^{\infty} f(E_F,\varepsilon)d\varepsilon \quad (A.2)$$

and the charge density for extended states is

$$\rho_E(r_i,z) = (-e)\left[\frac{m^*}{\pi\hbar^2}\right]^2 \int_{E_C}^{\infty} |\psi_\mu(r_i,z)|^2 \frac{L}{k_\perp} \int_{\varepsilon_\mu}^{\infty} f(E_F,\varepsilon)d\varepsilon d\varepsilon_\mu,$$
$$(A.3)$$

where $k_\perp = [2m^*(\varepsilon_\mu - E_C)/\hbar^2]^{1/2}$ and E_C is the CB minimum. The factor of L in Eq. (A.3) is a normalization length, which is cancelled by the factor of $1/L$ contained in the $|\psi_\mu|^2$ term of that equation. For states derived from a VB, the integrals extend from $-\infty$ to ε_μ or E_V, the Fermi-Dirac occupation factor $f(E_F,\varepsilon_\mu)$ becomes $1 - f(E_F,\varepsilon_\mu)$, the charge is $(+e)$, and $k_\perp = [2m^*(E_V - \varepsilon_\mu)/\hbar^2]^{1/2}$ where E_V is the VB maximum. The quantum-mechanical charge density is thusly given by

$$\rho_Q(r,z) = \rho_D[E_F - \phi(r,z)] + \rho_A[E_F - \phi(r,z)] + \rho_L(r,z)$$
$$+ \rho_E(r,z), \quad (A.4)$$

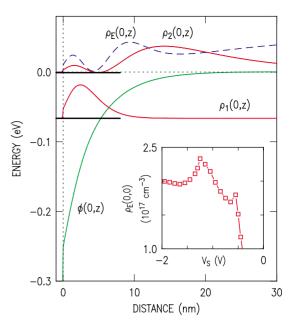where ρ_L and ρ_E are understood to include states from all

FIG. 6. (Color online) Electrostatic potential energy $\phi(0,z)$ and energies of localized states (heavy lines) relative to the CB minimum. Also shown are the charge densities of localized states $\rho_1(0,z)$ and $\rho_2(0,z)$, and the charge density of extended states $\rho_E(0,z)$. All quantities refer to their values along the central axis of the problem $r=0$ and are evaluated at a sample-tip voltage of -1.35 V. The inset shows $\rho_E(0,0)$ as a function of sample-tip voltage.

relevant bands. In practice, we use this charge density in the computations for z value in the semiconductor up to where the potential is negligible and the semiclassical result of Eq. (A.1) for larger z values. Self-consistency is obtained by iterating between this quantum charge density and the finite-element solution for the potential.

An example of our results is shown in Fig. 6, at a sample-tip voltage of -1.35 V for which there are two localized states (at 66 and 1 meV below E_C). The electrostatic potential energy in the semiconductor is shown, along with the charge densities of the localized states. Also shown is the total charge density of the extended states, $\rho_E(0,z)$. It should be noted that oscillations in this charge density occur near the surface, arising from the relatively large attractive potential at the surface. These oscillations persist even though the extended state charge density includes a summation of all occupied states in the CB. The Fermi level in our degenerately doped material is 46 meV above the CB minimum, so this summation of states extends over an energy range of that size (along with thermal broadening) but this range is not large compared to the potential-well depth of 251 meV at the surface.

The inset of Fig. 6 shows the extended state charge density evaluated at the surface, $\rho_E(0,0)$, as a function of sample-tip voltage. The sharp increase in this quantity for voltages extending down to -0.5 V corresponds to the formation of flat band conditions at the surface. The sharp drops seen in $\rho_E(0,0)$ at voltages of -0.6 and -1.3 V are due to the formation of localized states at these voltages. Actually, as these voltages are approached from above, the $\rho_E(0,z)$

curves display a significantly reduced magnitude for moderately large z values, leading finally to the formation of the localized states. This behavior gives rise to oscillations in the conductance of the extended states, Fig. 3(a). The self-consistency of the computations has only a relatively small effect on the results—if the semiclassical charge density of Eq. (A.1) is used, then the energies of the localized states and the shapes of the associated oscillations in Fig. 3(a) all change somewhat but the overall maximum magnitude of the conductance in the band-gap region is scarcely affected.

---

*feenstra@cmu.edu

[1] R. M. Feenstra and J. A. Stroscio, J. Vac. Sci. Technol. B **5**, 923 (1987).

[2] R. M. Feenstra, Phys. Rev. B **50**, 4561 (1994).

[3] R. Dombrowski, Chr. Steinebach, Chr. Wittneven, M. Morgenstern, and R. Wiesendanger, Phys. Rev. B **59**, 8043 (1999).

[4] R. Wiesendanger, *Scanning Probe Microscopy and Spectroscopy* (Cambridge University Press, Cambridge, England, 1994).

[5] R. M. Feenstra, G. Meyer, F. Moresco, and K. H. Rieder, Phys. Rev. B **66**, 165204 (2002).

[6] N. D. Jäger, E. R. Weber, K. Urban, and Ph. Ebert, Phys. Rev. B **67**, 165327 (2003).

[7] C. B. Duke, *Tunneling in Solids* (Academic, New York, 1969).

[8] D. Straub, M. Skibowski, and F. J. Himpsel, Phys. Rev. B **32**, 5237 (1985).

[9] R. M. Feenstra, Y. Dong, M. P. Semtsiv, and W. T. Masselink, Nanotechnology **18**, 044015 (2007).

[10] Y. Dong, R. M. Feenstra, M. P. Semtsiv, and W. T. Masselink, J. Appl. Phys. **103**, 073704 (2008).

[11] R. M. Feenstra, J. Vac. Sci. Technol. B **21**, 2080 (2003).

[12] J. Bardeen, Phys. Rev. Lett. **6**, 57 (1961).

[13] R. M. Feenstra, J. Y. Lee, M. H. Kang, G. Meyer, and K. H. Rieder, Phys. Rev. B **73**, 035310 (2006).

[14] R. M. Feenstra, S. Gaan, G. Meyer, and K. H. Rieder, Phys. Rev. B **71**, 125316 (2005).

[15] K. C. Pandey, J. Vac. Sci. Technol. **15**, 440 (1978).

[16] I. Vurgaftman, J. R. Meyer, and L. R. Ram-Mohan, J. Appl. Phys. **89**, 5815 (2001).

[17] B. Engels, P. Richard, K. Schroeder, S. Blügel, Ph. Ebert, and K. Urban, Phys. Rev. B **58**, 7799 (1998).

[18] For extended states, the integral is performed far into the semiconductor where the potential is negligible and the wave function are matched to appropriate traveling waves in the bulk semiconductor. For localized states, the integral is performed similarly far into the semiconductor and the occurrence of a localized state corresponds to the situation when the wave function obtained from the integration goes to zero (as opposed to diverging) at this large value of z.